Superior optical ($\lambda \sim 1550$ nm) emission and detection characteristics of Ge microdisks grown on virtual $Si_{0.5}Ge_{0.5}$/Si substrates using molecular beam epitaxy

Sudarshan Singh[1], Ajit K Katiyar[1], Arijit Sarkar[2], P K Shihabudeen[3], Ayan Roy Chaudhuri[2,3], Dipak K Goswami[1] and Samit K Ray[1,4]

[1] Department of Physics, Indian Institute of Technology, Kharagpur—721302 Kharagpur, India
[2] Advanced Technology Development Centre, Indian Institute of Technology, Kharagpur—721302 Kharagpur, India
[3] Materials Science Centre, Indian Institute of Technology, Kharagpur—721302 Kharagpur, India
[4] S. N. Bose National Centre for Basic Sciences, Kolkata 700106, India

E-mail: physkr@phy.iitkgp.ac.in

Abstract

We report the optical characteristics of relatively large sized (∼7.0–8.0 μm) but low aspect ratio Ge microdisks grown on a virtual $Si_{0.5}Ge_{0.5}$ substrate using molecular beam epitaxy following the Stranski–Krastanov growth mechanism. Grown microdisks with very low aspect ratio Ge islands exhibit direct band gap (∼0.8 eV) photoluminescence emission sustainable up to room temperature, enabled by the confinement of carriers into the microdisks. *p–i–n* diodes with an intrinsic layer containing Ge microdisks have been fabricated to study their emission and photoresponse characteristics at an optical communication wavelength of ∼1550 nm. A strong electroluminescence at 1550 nm has been achieved at low temperatures in the device for a very low threshold current density of 2.56 $\mu A\ cm^{-2}$ due to the strong confinement of injected holes. The emission characteristics of the fabricated device with respect to the injected current density and temperature have been studied. Novel emission and optical modulation characteristics at 1550 nm of the fabricated *p–i–n* device containing Ge microdisks grown on a virtual SiGe substrate indicate its potential for Si CMOS compatible on-chip optical communications.

Keywords: molecular beam epitaxy, virtual SiGe substrate, SK growth mode, Ge microdisks, photoluminescence, *p–i–n* devices, electroluminescence

1. Introduction

Significant progress has been made towards implementing silicon (Si) photonics and optical interconnects for on-chip communication [1]. Results have been reported on high performance Si-compatible detectors, modulators and emitters for the near and mid-infrared (IR) region [2–7]. However, the integration of low-cost optoelectronic systems working in an optical-communication wavelength range of 1.3–1.55 μm is a major challenge [8]. Germanium is a primary choice of interest for such devices because of its compatibility with complementary metal oxide semiconductor (CMOS) technology and its direct optical band gap in the communication band, which is slightly above its indirect band gap. Recently, several approaches, such as quantum confinement [9, 10], strain engineering [11, 12] and alloying with Sn [13, 14],

have been explored to achieve the emission and detection at an optical communication wavelength using Ge. The growth of Ge islands on Si in a self-assembled manner following the Stranski–Krastanov (SK) growth mechanism is a promising approach, resulting in a tunable band gap by utilizing the quantum confinement effect [15]. Although Ge possesses a distinct advantage for the ease of integration on Si over III–V semiconductors for light detection in the telecommunication band [8], the thermionic emission and high dislocation density due to large lattice mismatch between the two materials limit the overall performance of Ge/Si-based photodiodes. Theoretical models along with experimental approaches have been reported to understand and optimize the growth condition of Ge/Si heterostructures to improve the photodiode characteristics [16, 17]. To achieve a high-quality Ge on Si with reduced dislocation density, several new strategies have been employed by researchers [18–22]. Fitzgerald *et al* [23] reported a significant reduction in threading dislocation density using an optimized relaxed SiGe (RSG) graded buffer layer as a substrate followed by a chemical mechanical polishing and demonstrated a Ge *p–n* photodiode on Si substrate working at 1.3 μm with a moderate dark current density. However, the fabricated device was useful only for optical detection. On the other hand, a complex and expensive device fabrication process is required [24] to achieve an intense injected carrier-induced emission in the communication wavelength using the Si/Ge system. Micro-cavities [25] and microdisk resonators [26] have been used in order to achieve strong resonant luminescence intensity. Owing to the advantage of reduced lattice mismatch between a Ge overlayer on RSG substrates, the growth of strain-relaxed, larger-sized Ge islands on virtual substrates is possible, which can be useful for Ge-based emitters and detectors. However, the applications of reported devices working in the communication band are still limited in terms of their solo performance, either in detection or emission.

Here, we report for the first time the room temperature emission and detection characteristics from single-layer self-assembled Ge microdisks grown on fully strain-relaxed SiGe virtual substrates using molecular beam epitaxy (MBE) following the SK growth mode. The effect of temperature on the light emission characteristics of grown Ge microdisks has been analyzed. For device demonstration, a *p–i–n* diode structure has been fabricated using grown Ge microdisks sandwiched between the p-Si substrate and a high band gap n-Al doped ZnO (AZO) film working as an optically-transparent but electrically conducting layer. The incident optical power-dependent photoresponse and injected current-induced emission from the fabricated *p–i–n* diode at communication wavelength (~1550 nm) are reported.

2. Experimental section

Germanium microdisks were grown inside a MBE system (SVT Associates, Inc.) on commercially procured fully strain-relaxed $Si_{0.5}Ge_{0.5}$ (RSG) substrates. RSG substrates used in the present study were fabricated by depositing a graded film of Ge on p-Si (100) substrate with varying content from 0%–50% over a thickness of 5.4 μm and the growth of 1.54 μm thick film of $Si_{0.5}Ge_{0.5}$ on top using chemical vapour deposition. RSG substrates were cleaned *ex situ* by dipping in 1% hydrofluoric solution for 2 min prior to insertion into the MBE system. The growth of the Ge microdisks was performed at two different substrate temperatures of 400 °C and 500 °C by keeping the growth rate constant at 0.1 nm s^{-1}. The MBE system utilized a Knudsen cell for the growth of nominally undoped Ge. The growth was performed at a chamber pressure of $<2 \times 10^{-10}$ mbar using a combination of cryo and ion pumps. The surface morphology of the samples was studied using atomic force microscopy (AFM) in tapping mode (Veeco Nanoscope-IV), field-emission scanning electron microscopy (FESEM) (ZEISS SUPRA 40 microscope) and transmission electron microscopy (TEM) (JEOL JEM-2100F microscope). The temperature-dependent near IR photoluminescence (PL) spectra were recorded with a synchronized lock-in technique, where the excitation laser beam (980 nm) was mechanically chopped at a frequency of 172 Hz and the emission was measured using a Triax-320 monochromator having a cryo-cooled InGaAs detector. To investigate the electroluminescence (EL) characteristics of the grown microdisks, we fabricated *p–i–n* light emitting diode (LED) devices. For the fabrication of the *p–i–n* LED, a thin AZO film (~20 nm) as the n-type layer was deposited under an optimized condition by pulsed laser deposition, while Ge islands acted as an intrinsic layer with a p-type substrate. The top (Au) and bottom (Al) electrodes were deposited by a thermal evaporation process. Room temperature photodetection measurements of the device were carried out using a Keithley 4200-SCS semiconductor parameter analyzer. The photoconductivity spectrum was recorded using a Newport quantum efficiency measurement system equipped with a broad-band light source, a lock-in amplifier and a monochromator. For measurements at infrared spot wavelengths, a 1310 nm laser diode (FPL1053T) and a 1550 nm Fabry–Perot bench top laser source (S4FC1550, Thorlabs) were used. The transient photocurrent measurement was performed using a 980 nm diode laser (LQC980-220E, Newport), which was modulated using an external function generator (Agilent 33521A) with 50% duty cycle and recorded with a digital oscilloscope (Tektronix-TBS1202B).

3. Results and discussion

For heteroepitaxial systems, the strain-driven growth of self-assembled islands has become an attractive route for the integration of coherent nanoislands for the fabrication of optoelectronic devices. The substrate temperature, lattice mismatch, and growth rate are the key parameters in determining the size and shape of the islands grown under the SK mode as well as the resultant device performance. In the SK growth mode, the mechanism of island growth is strain-driven where the existing strain is determined by the lattice or composition mismatch between the epilayer and substrate. It has been reported that islands grown on $Ge_{0.8}Si_{0.2}$/Si (001)

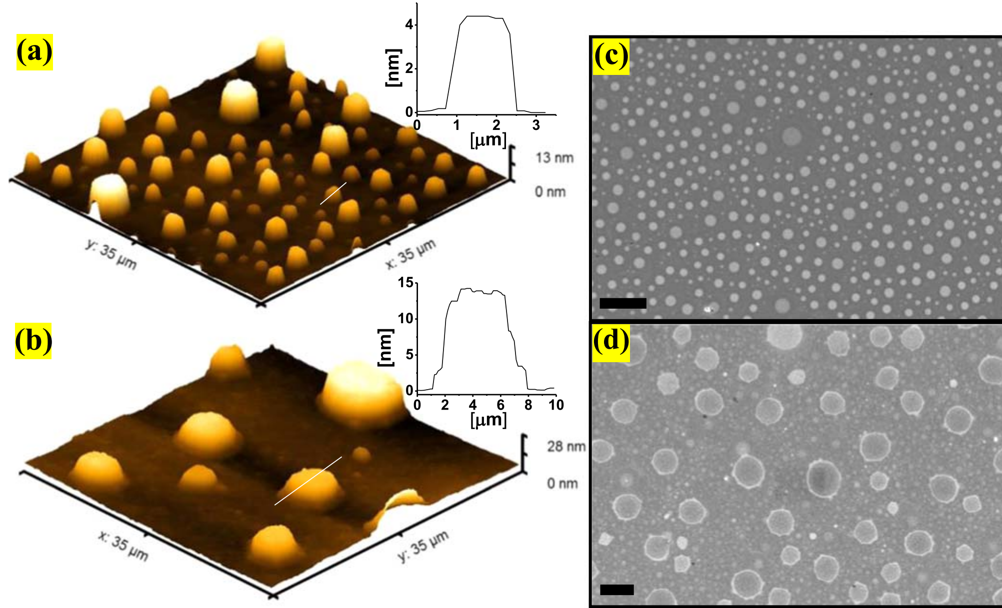

Figure 1. 3D topographic AFM images of Ge microdisks recorded in tapping mode and the height profile of a single microdisk (inset), grown on RSG substrates at a growth temperature of (a) 400 °C and (b) 500 °C and corresponding FESEM micrographs (c) and (d) with 10 μm scale bar.

result in a much larger size in comparison to the Ge/Si (001) system, implying that the substrate composition strongly affects the size and shape [27]. The strain energy near the base increases during the lateral growth of islands until it compensates the growth driving force, which leads to the cessation of the island width at this instance. So the use of a relaxed SiGe virtual substrate with a higher Ge concentration allows the high-quality growth of larger-sized Ge islands with reduced threading dislocation density, which may be useful for applications in emission and detection devices.

MBE growth was performed at different substrate temperatures, keeping the Ge cell temperature (1150 °C) and growth time constant. The lateral size and height of the Ge islands are found to increase with an increase in growth temperature. Typical three-dimensional (3D) AFM surface topo-graphs of the samples grown at 400 °C and 500 °C on RSG virtual substrate are depicted in figures 1(a) and (b), respectively. AFM images reveal that Ge islands, grown at both temperatures, exhibit a microdisk-like shape with a very low aspect ratio, rather than the formation of pyramid or dome-type structures reported on Si(100) substrates [28, 29]. Abstreiter *et al* [30] reported a systemic study on the effect of temperature and flux rate on the size and density distribution of self-assembled Ge quantum dots grown on Si and found that the average island size increases with an increase in deposition temperature or reduction in Ge flux. As shown in the AFM micrographs in figures 1(a) and 1(b), Ge islands of a larger diameter appear along with some smaller ones, revealing a bimodal size distribution. The average diameter and vertical height of these microdisk-like Ge islands has been calculated from AFM micrographs at different regions for both samples. Ge microdisks grown at 400 °C exhibit diameters in the range of ~1.0–2.0 μm with an average vertical height of ~4.0 ± 0.5 nm, whereas those grown at 500 °C exhibit a height of ~12.0 ± 2.0 nm for larger diameter islands (size ~7.0–8.0 μm). To represent the average vertical height of the grown microdisks, the typical height profile of a single Ge microdisk with an average diameter for both the samples is presented in the insets of figures 1(a) and (b), respectively. It may be noted that the average vertical dimension of the microdisks in both samples is below the excitonic Bohr radius of Ge (~24 nm), making them attractive for carrier confinement in the growth direction and the fabrication of optical devices.

Figures 1(c) and (d) represent the FESEM images of Ge islands grown at 400 °C and 500 °C, respectively. The images reveal that the bifurcation of the size of the Ge islands does not occur at a substrate temperature of 400 °C showing an average island diameter in between 1.0–2.0 μm. But, the sample grown at 500 °C clearly reveals the formation of two distinct families of islands, one with an average diameter between ~1.0–2.0 μm and the other with ~7.0–8.0 μm. This kind of clear bifurcation in the size distribution of self-assembled Ge nanocrystals at a certain growth condition in Ge/Si systems has been reported by several groups, including us [31–33]. The size distribution of smaller Ge microdisks for both the growth temperatures of 400 °C and 500 °C can be ascribed to the nucleation of 3D islands in order to compensate the strain energy, whereas the growth of microdisks with a larger diameter at 500 °C is attributed to the Ostwald ripening controlled coarsening process, resulting in the growth of larger-sized microdisks at the expense of smaller ones due to the ad-atom concentration difference between different-sized islands at a higher growth temperature [34]. Since larger diameter Ge islands with a height lower than the excitonic Bohr radius are attractive for the fabrication of a single microdisk-based cavity and waveguided photonic devices, we adopted the 500 °C grown samples for the optical

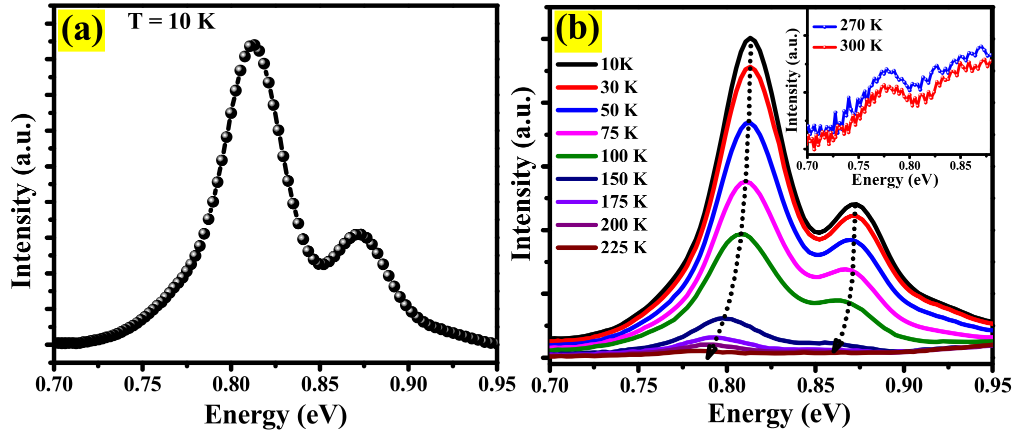

Figure 2. (a) Photoluminescence spectra of Ge microdisks grown at 500 °C and recorded at 10 K showing the direct band gap transition from Ge. (b) Corresponding temperature-dependent PL spectra at an excitation power of 87 mW with the inset showing the emission at 270 and 300 K.

characteristic investigation and device fabrication in this work. Samples grown above ∼500 °C were not considered for further measurements in the present study due to the larger height of the microdisks and significant Si–Ge intermixing [35].

In order to investigate the strain relaxation in Ge microdisks grown on RSG substrates for both growth temperatures, we have performed high resolution x-ray rocking curve measurements around (004) and (224) Bragg planes. Figure S1 (supplementary information available online at stacks.iop.org/NANO/31/115206/mmedia) depicts the rocking curve spectra of the RSG substrate and Ge microdisks grown at 500 °C around the (004) Bragg plane. A sharp peak is attributed to the diffraction from the Si (004) plane, whereas the broader one at a lower Bragg angle side represents a combination of variable Ge content in the RSG substrate and microdisks. The absence of a separate peak corresponding to the Ge microdisks in the rocking curve data indicates that the islands grown at 500 °C on a virtual substrate are completely strain relaxed. The composition gradient of Ge in the virtual substrate results in a broader Bragg peak due to Ge. However, the peak broadening after the growth of the Ge microdisks has been found to be reduced in comparison to the RSG substrate, which is attributed to the improved crystalline quality of the graded layer at an elevated substrate temperature due to recrystallization.

The PL spectrum of larger diameter Ge microdisks grown at 500 °C, recorded at 10 K with an excitation power of 87 mW, is illustrated in figure 2(a). An intense emission band centered at ∼0.81 eV is attributed to the direct band-to-band radiative transition of electrons due to the quantum confinement of carriers in the growth direction of Ge microdisks. The obtained PL data are in excellent agreement with the reported theoretically calculated band gap energy of ∼0.81 eV for a ∼12 nm thick Ge quantum well structure [36]. A relatively large full-width-half-maximum of the PL peak may be attributed to the size distribution of the Ge islands. Furthermore, a broad emission band towards the higher energy side with an emission peak at ∼0.87 eV is attributed to the top $Si_{0.5}Ge_{0.5}$ relaxed layer of the RSG virtual substrate [11, 37, 38]. Figure 2(b) represents the temperature-dependent (temperature range: 10–300 K) PL spectra of Ge microdisks grown at 500 °C. The effect of temperature on the PL spectra is noticeable as a drop in the emission intensity at a higher temperature along with a clear red shift in the peak position. The emission from the band-to-band transition is clearly observed even at a temperature up to 300 K (inset of figure 2(b)). The decrement in intensity is owing to the thermal quenching of the radiative recombination efficiency at an elevated temperature. The PL quenching at higher temperatures is associated with carrier migration from localized states and the activation of the non-radiative recombination centres, which eventually reduces the emission intensity by increasing the phonon or defect-mediated transition. The observed room temperature PL from the microdisks of the Ge grown on RSG substrates appears attractive for fabricating optical sources at a communication wavelength of 1550 nm.

We measured the room temperature photoconductivity characteristics of single layer Ge microdisks (grown at 500 °C) in the wavelength range starting from 500 nm–1550 nm. The photocurrent measurement of the fabricated *p–i–n* device has been performed in photovoltaic mode at room temperature under a normal incidence configuration. Figure S2(a) (supplementary information) represents the broad-band photoconductivity spectra of the fabricated device for a continuous wavelength ranging from 500 nm–1100 nm. The device also exhibits a significant change in conductivity under illumination at a spot IR wavelength of 1310 nm, as shown in figure S2(b). The observed photocurrent at the near IR region and 1310 nm is attributed to the silicon underneath and the graded Ge film in the RSG substrate, respectively. Figure 3(a) depicts the photocurrent response of the Ge microdisks under illumination at a wavelength of 1550 nm. A sharp enhancement in the current is clearly observed under illumination of light (ON state), which immediately switches back to a lower conductivity state (OFF state) under dark conditions. On the other hand, the control device fabricated without Ge microdisks does not exhibit any change in conductivity under illumination, as shown in the inset of figure 3(a). The control experiment clearly demonstrates that Ge microdisks, grown

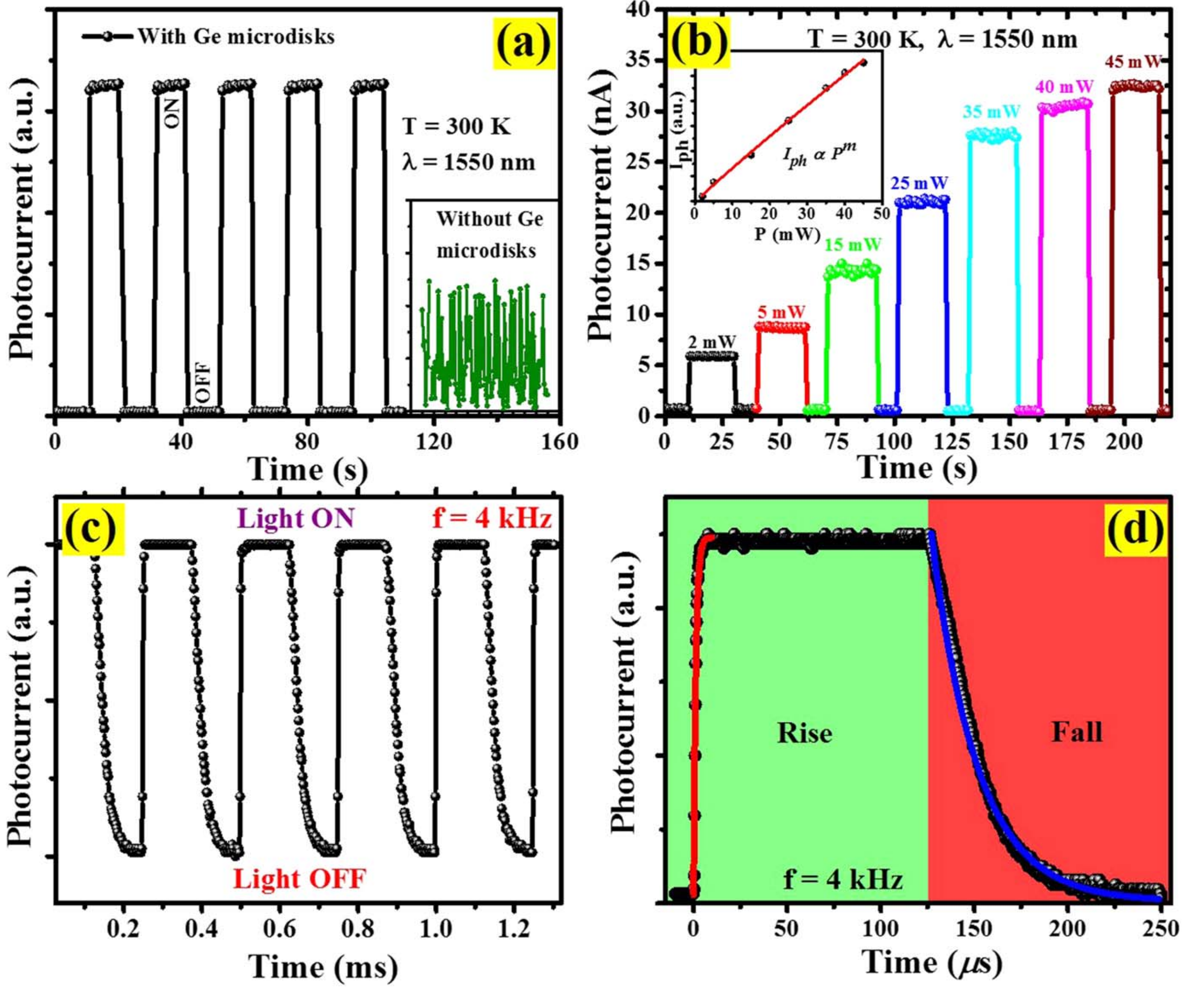

Figure 3. (a) Photoresponse characteristics of Ge microdisks at an excitation wavelength of 1550 nm and the inset shows the photoresponse of a control device without Ge microdisks. (b) Dynamic photoresponse of the fabricated device with Ge microdisks at 1550 nm as a function of incident optical power and the fitted curve using the power law (inset). (c) Transient photocurrent of the fabricated photoconductive device at a wavelength of 980 nm modulated at a frequency of 4 kHz. (d) Rise and fall times of the device estimated at 4 kHz.

Table 1. Comparison of the responsivity of Ge QD-based photodetectors reported in the literature.

Active region	Diode design	Responsivity (mAW^{-1})	References
3 layers of Ge QDs/Si	*p–i–n* RCE-PD	1.25 @ −5 V	[42]
10 layers of Ge QDs/Si	*p–i–n*	.004 @4 V	[43]
10 layers of Ge QDs/Si	MOSFET	.5 @ $V_{DS} = 6$ V	[44]
20 layers GDs/SiGe layer	*p–i–n*	3 @ 0 V	[45]
30 layers Ge QDs/Si	*p–i–n*	1 @ 0 V	[46]
Multiple layer Ge QDs (MQW)	SOI-based RCE-PD	0.03	[47]
Single layer of Ge QDs	***p–i–n***	**0.13 @ 0 V**	**This work**

on RSG substrates under SK growth mode, only contribute to the observed photocurrent at 1550 nm. The direct band-to-band absorption (∼0.8 eV) in the Ge microdisks at 1550 nm results in photogenerated carriers, which enhances the current through the device. The responsivity of the fabricated device at 1550 nm is found to be ∼0.13 mA W^{-1}. The responsivity value of the device fabricated with single layer microdisk-like Ge islands is comparable to the devices reported with multi-layer Ge QDs/Si structures. Table 1 illustrates the comparison of reported responsivity values from the literature. The room temperature optical response under the illumination of vertically-confined Ge microdisks is potentially attractive for

on-chip optical detection. Therefore, the dynamic photoresponse observed from Ge microdisks under 1550 nm laser illumination with the power varying from 2–45 mW at zero bias was measured and is presented in figure 3(b). With an increase in the optical power (P), an enhancement in the photocurrent (I_{ph}) is observed, which can be fitted using a power law relation, $I_{ph} \propto P^m$. The exponent 'm' is found to be near unity (0.91), indicating a sub-linear dependence of the photocurrent, which can be ascribed to the presence of localized traps near the band edges, resulting in some recombination of photogenerated carriers [39]. In order to investigate the optical switching characteristics of the fabricated device, the transient photocurrent has been recorded under an illumination of 980 nm pulsed light modulated at a frequency of 4 kHz (figure 3(c)). We have calculated the rise (t_r) and fall (t_f) time by fitting the rise and decay profile of a single pulse using the following exponential equations [40], respectively:

$$I_r = I_0 - I_0 \times e^{\left(-\frac{t}{t_r}\right)} \tag{1}$$

$$I_f = I_0 + A_1 \times e^{\left(-\frac{t}{t_f}\right)} \tag{2}$$

where I_0 is the initial current, I_r and I_f represent the currents as a function of time during the rise and fall of the transients in the sub-cycle, respectively, whereas A_1 is an independent variable and t is the elapsed time. For illustration, a single cycle at a frequency of 4 kHz with fitted data is presented in figure 3(d) and the rise and fall times are estimated to be around ~1 μs and ~24 μs, respectively. The observed response time of the fabricated device is comparable to commercially available Si/Ge detectors (918D, Newport). The change in the photocurrent under illumination within a few μs makes these devices attractive for optical modulators.

The study of EL characteristics under the electrical injection of carriers is essential to test the efficacy of Ge microdisks for Si compatible optical sources. Figure 4(a) depicts the schematic structure of the fabricated Ge microdisk-based *p–i–n* LED along with an optical image (inset of figure 4(a)). Typical *I–V* characteristics of the fabricated *p–i–n* diode at 10 K are presented in figure 4(b). The fabricated device exhibits an excellent rectifying behaviour with a sharp increment in current density above 7.5 V under a forward bias condition. The inset of figure 4(b) illustrates the energy band diagram of the device representing different electronic transitions for EL emission under a forward bias. On applying a bias, the injected holes through the Si side accumulate within the Ge islands due to a large valence band offset (~2.9 eV) between Ge and AZO [41]. A strong confinement of holes leads to the radiative recombination with injected electrons from AZO within the Ge islands, resulting in an emission around 1550 nm. To examine the role of the large valance band offset between Ge and AZO in the electronically-induced emission, we have fabricated a control device without AZO films. No emission, even at a temperature of 10 K, is observed from the device without AZO films, as shown in figure S3 (supplementary information). The EL spectra of the *p–i–n* diode as a function of injected current density, recorded at a constant temperature of 10 K, is depicted in figure 4(c) and a threshold current density for the emission is found to be 2.56 μA cm^{-2} (shown in the inset). All the EL spectra display two distinct emission peaks centered at ~0.81 eV and ~0.87 eV. The observed EL peaks are in excellent agreement with the PL spectra observed at 10 K. The emission peak at ~0.81 eV is attributed to the radiative recombination of injected carriers in the active region consisting of Ge microdisks, whereas the one centered at ~0.87 eV is ascribed to the transverse optical phonon-assisted transition in the $Si_{0.5}Ge_{0.5}$ relaxed layer in the RSG substrates [37]. The emission intensity for both the transitions increases with an increase in the injected current density. The effect of sample temperature on the EL spectra, recorded at a constant injection current density of 6.30 mA cm^{-2}, has been studied and the results are depicted in figure 4(d). The EL intensity of the fabricated device decreases with an increase in temperature. However, a detectable EL intensity of 1550 nm emission is observed, even at 100 K (inset of figure 4(d)). The non-radiative trap centres present at the interfaces in both sides of the Ge microdisks may be responsible for the thermal quenching of the EL intensity at elevated temperatures. However, the observed current-induced emission above the liquid nitrogen temperature from single-layer self-assembled Ge microdisks grown on RSG substrates demonstrates its potential for Si CMOS compatible sources in the optical communication wavelength.

4. Conclusions

In conclusion, we have grown relatively large diameter but very low aspect ratio Ge microdisks on strain-relaxed virtual $Si_{0.5}Ge_{0.5}$/Si substrates using molecular beam epitaxy and studied their efficacy for the first time for applications in both optical communication sources and detectors. The reduced lattice mismatch between the Ge and RSG substrate results in the formation of relatively larger diameter strain-relaxed microdisks with a height (4–12 nm) lower than the excitonic Bohr radius of Ge. This has led to the observation of direct band gap PL emission from Ge microdisks even up to room temperature. Furthermore, we have demonstrated optical emission and detection in the telecommunication wavelength (~1550 nm) by fabricating *p–i–n* diode structures using single-layer self-assembled Ge microdisks. Power-dependent optical modulation at 1550 nm and switching transients of the *p–i–n* diode at zero bias under 980 nm illumination are presented. The current-induced direct band-to-band EL emission observed above liquid nitrogen temperature (up to 100 K) from the fabricated device confirms its potential for an optical source at the telecommunication wavelength. Thus, large diameter, low aspect ratio, strain-free Ge microdisks grown on virtual SiGe substrates appear attractive towards the realization of Si CMOS compatible on-chip optical devices operating at the communication band.

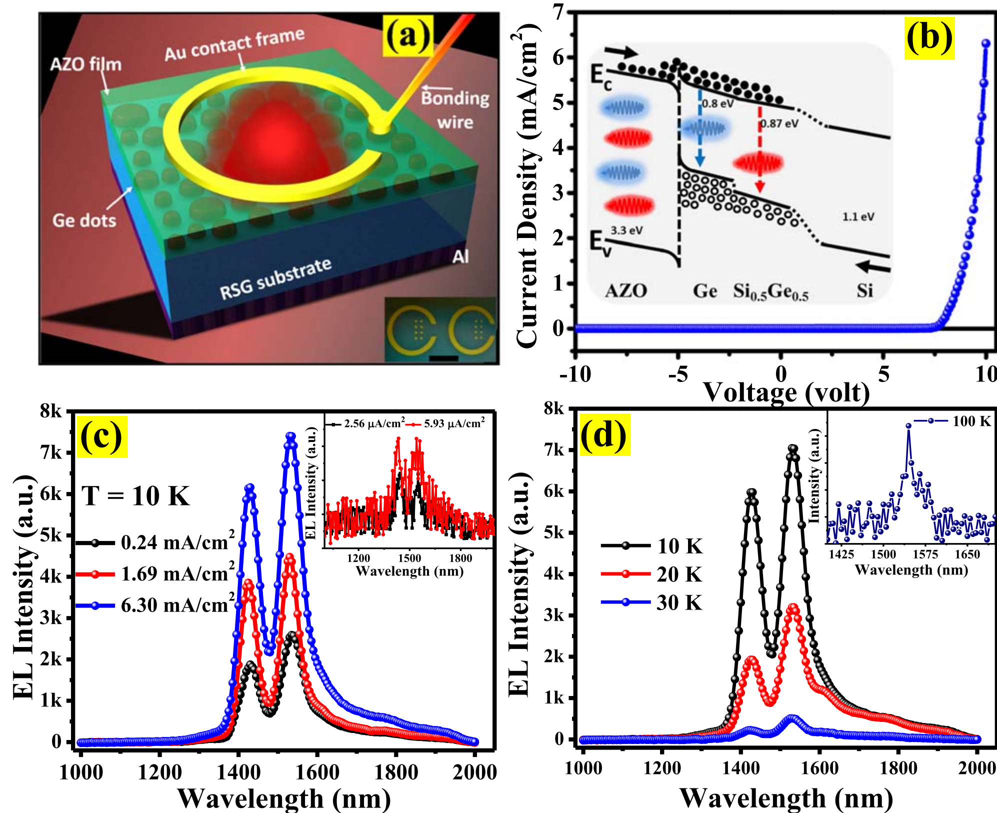

Figure 4. (a) A schematic layout and an optical image (inset) of the fabricated light emitting device with 3 mm scale bar. (b) Typical *I–V* characteristics of the device recorded at 10 K and the inset shows the energy band alignment of the device illustrating different radiative transitions for EL emission under forward bias. (c) EL spectra of the fabricated device as a function of injected current density at 10 K. The inset of figure (c) shows the onset of emission at an injected current density of 2.56 μA cm^{-2}. (d) The EL intensity as a function of temperature at a constant injected current density of 6.30 mA cm^{-2} and the spectrum at 100 K is shown in the inset.

Acknowledgments

We would like to acknowledge the financial support from Meity & DST sponsored NNETRA (Grant No. 5(1)/2017-NANO) and MHRD-DRDO IMPRINT (Grant No. 3-18/2015-T.S.-I (Vol. IV)) projects of the Government of India. The use of the cluster MBE facility established under the Deity sponsored project at ATDC, IIT Kharagpur is gratefully acknowledged. The authors would also like to acknowledge Dr Rajshekhar Bar for help with the HR-XRD measurements.

ORCID iDs

Samit K Ray https://orcid.org/0000-0002-8099-6690

References

[1] Pavesi L and Guillot G 2006 *Optical Interconnects: The Silicon Approach* (Berlin: Springer)

[2] Eng P C, Song S and Ping B 2015 State-of-the-art photodetectors for optoelectronic integration at telecommunication wavelength *Nanophotonics* **4** 277–302

[3] Reed G T, Mashanovich G, Gardes F Y and Thomson D J 2010 Silicon optical modulators *Nat. Photonics* **4** 518–26

[4] Gallacher K, Velha P, Paul D J, Cecchi S, Frigerio J, Chrastina D and Isella G 2012 1.55 μm direct bandgap electroluminescence from strained n-Ge quantum wells grown on Si substrates *Appl. Phys. Lett.* **101** 211101

[5] Ray S K, Maikap S, Banerjee W and Das S 2013 Nanocrystals for silicon-based light-emitting and memory devices *J. Phys. D. Appl. Phys.* **46** 153001

[6] Oehme M, Gollhofer M, Widmann D, Schmid M, Kaschel M, Kasper E and Schulze J 2013 Direct bandgap narrowing in Ge LED's on Si substrates *Opt. Express* **21** 2206

[7] Timofeev V, Nikiforov A, Yakimov A, Mashanov V, Loshkarev I, Bloshkin A, Kirienko V, Novikov V and Kareva K 2019 Studying the morphology, structure, band diagram of thin GeSiSn films and their mid-infrared photoresponse *Semicond. Sci. Technol.* **34** 14001

[8] Michel J, Liu J and Kimerling L C 2010 High-performance Ge-on-Si photodetectors *Nat. Photonics* **4** 527–34

[9] Fei E T *et al* 2015 Investigation of germanium quantum-well light sources *Opt. Express* **23** 22424

[10] Kuo M H, Chou S K, Pan Y W, Lin S D, George T and Li P W 2016 'Embedded emitters': direct bandgap Ge nanodots within SiO_2 *J. Appl. Phys.* **120** 233106

[11] Katiyar A K, Grimm A, Bar R, Schmidt J, Wietler T, Osten H J and Ray S K 2016 Room temperature direct band gap emission characteristics of surfactant mediated grown compressively strained Ge films *Nanotechnology* **27** 435204

[12] Liu J *et al* 2005 High-performance, tensile-strained Ge p-i-n photodetectors on a Si platform *Appl. Phys. Lett.* **87** 103501

[13] Kim S, Bhargava N, Gupta J, Coppinger M and Kolodzey J 2014 Infrared photoresponse of GeSn/n-Ge heterojunctions grown by molecular beam epitaxy *Opt. Express* **22** 11029

[14] Bar R, Katiyar A K, Aluguri R and Ray S K 2017 Emission characteristics of self-assembled strained Ge_{1-x} Sn_x islands for sources in the optical communication region *Nanotechnology* **28** 295201

[15] Wang K L, Cha D, Liu J and Chen C 2007 Ge/Si Self-assembled quantum dots and their optoelectronic device applications *Proc. IEEE* **95** 1866–83

[16] Izhnin I I, Fitsych O I, Voitsekhovskii A V, Kokhanenko A P, Lozovoy K A and Dirko V V 2018 Nanostructures with Ge–Si quantum dots for infrared photodetectors *Opto-Electron. Rev.* **26** 195–200

[17] Lozovoy K A, Voitsekhovskii A V, Kokhanenko A P and Satdarov V G 2015 Photodetectors and solar cells with Ge/Si quantum dots parameters dependence on growth conditions *Int. J. Nanotechnol.* **12** 209–17

[18] Luryi S, Kastalsky A and Bean J C 1984 New infrared detector on a silicon chip *IEEE Trans. Electron Devices* **31** 1135–9

[19] Fitzgerald E A 1991 Dislocations in strained-layer epitaxy: theory, experiment, and applications *Mater. Sci. Reports* **7** 87–142

[20] Luan H-C, Lim D R, Lee K K, Chen K M, Sandland J G, Wada K and Kimerling L C 1999 High-quality Ge epilayers on Si with low threading-dislocation densities *Appl. Phys. Lett.* **75** 2909–11

[21] Choi D, Ge Y, Harris J S, Cagnon J and Stemmer S 2008 Low surface roughness and threading dislocation density Ge growth on Si (001) *J. Cryst. Growth* **310** 4273–9

[22] David T, Aqua J, Liu K, Favre L, Ronda A, Abbarchi M, Claude J and Berbezier I 2018 New strategies for producing defect free SiGe strained nanolayers *Sci. Rep.* **8** 2891

[23] Samavedam S B, Currie M T, Langdo T A and Fitzgerald E A 1998 High-quality germanium photodiodes integrated on silicon substrates using optimized relaxed graded buffers *Appl. Phys. Lett.* **73** 2125–7

[24] Boucaud P *et al* 2013 Recent advances in germanium emission [Invited] *Photonics Res.* **1** 102

[25] Xia J S, Ikegami Y, Shiraki Y, Usami N and Nakata Y 2006 Strong resonant luminescence from Ge quantum dots in photonic crystal microcavity at room temperature *Appl. Phys. Lett.* **89** 201102

[26] Shambat G, Cheng S-L, Lu J, Nishi Y and Vuckovic J 2010 Direct band Ge photoluminescence near 1.6 μm coupled to Ge-on-Si microdisk resonators *Appl. Phys. Lett.* **97** 241102

[27] Liao X Z, Zou J, Cockayne D J H, Jiang Z M, Wang X and Leon R 2000 Composition and its impact on shape evolution in dislocated Ge(Si)/Si islands *Appl. Phys. Lett.* **77** 1304–6

[28] Singha R K, Manna S, Das S, Dhar A and Ray S K 2010 Room temperature infrared photoresponse of self assembled Ge/Si (001) quantum dots grown by molecular beam epitaxy *Appl. Phys. Lett.* **96** 233113

[29] Singha R K, Das S, Majumdar S, Das K, Dhar A and Ray S K 2008 Evolution of strain and composition of Ge islands on Si (001) grown by molecular beam epitaxy during postgrowth annealing *J. Appl. Phys.* **103** 114301

[30] Abstreiter G, Schittenhelm P, Engel C, Silveira E, Zrenner A, Meertens D and Jäger W 1996 Growth and characterization of self-assembled Ge-rich islands on Si *Semicond. Sci. Technol.* **11** 1521–8

[31] Williams R S, Medeiros-Ribeiro G, Kamins T I and Ohlberg D A A 1999 Chemical thermodynamics of the size and shape of strained Ge nanocrystals grown on Si(001) *Acc. Chem. Res.* **32** 425–33

[32] Medeiros-Ribeiro G, Bratkovski A M, Kamins T I, Ohlberg D A A and Williams R S 1998 Shape transition of germanium nanocrystals on a silicon (001) surface from pyramids to domes *Science* **279** 353–5

[33] Das S, Manna S, Singha R K, Aluguri R and Ray S K 2013 Effect of growth temperature and post-growth annealing on luminescence properties of molecular beam epitaxy grown single layer Ge quantum dots *J. Appl. Phys.* **113** 63101

[34] Ross F M, Tersoff J and Tromp R M 1998 Coarsening of self-assembled Ge quantum dots on Si(001) *Phys. Rev. Lett.* **80** 984–7

[35] Valvo M, Bongiorno C, Giannazzo F and Terrasi A 2013 Localized Si enrichment in coherent self-assembled Ge islands grown by molecular beam epitaxy on (001)Si single crystal *J. Appl. Phys.* **113** 033513

[36] Lin G, Chen N, Zhang L, Huang Z, Huang W, Wang J, Xu J, Chen S and Li C 2016 Room temperature electroluminescence from tensile-strained $Si_{0.13}Ge_{0.87}$/Ge multiple quantum wells on a Ge virtual substrate *Materials* **9** 803

[37] Manna S, Aluguri R, Das S, Singha R and Ray S K 2013 Electroluminescence from metal-insulator-semiconductor tunneling diodes using compressively strained Ge on $Si_{0.5}Ge_{0.5}$ virtual substrates *Opt. Express* **21** 28219

[38] Schittenhelm P, Gail M and Abstreiter G 1995 Self-organized MBE growth of Ge-rich SiGe dots on Si(100) *J. Cryst. Growth* **157** 260–4

[39] Mukherjee S, Das K, Das S and Ray S K 2018 Highly responsive, polarization sensitive, self-biased single GeO_2-Ge nanowire device for broadband and low power photodetectors *ACS Photonics* **5** 4170–8

[40] Hossain M, Kumar G S, Barimar Prabhava S N, Sheerin E D, McCloskey D, Acharya S, Rao K D M and Boland J J 2018 Transparent, flexible silicon nanostructured wire networks with seamless junctions for high-performance photodetector applications *ACS Nano* **12** 4727–35

[41] Yun J-H, Kumar M D, Patel M, Park Y C, Byung S K and Kim J 2016 Transparent conductor-embedding high-sensitive germanium NIR photodetector *Mater. Sci. Semicond. Process.* **48** 95–100

[42] Xu X, Chiba T, Maruizumi T and Shiraki Y 2014 Microdisk enhanced photodetector based on Ge self-assembled quantum dots on silicon-on-insulator *Thin Solid Films* **557** 363–7

[43] Elfving A, Hansson G V and Ni W X 2003 SiGe (Ge-dot) heterojunction phototransistors for efficient light detection at 1.3–1.55 μm *Physica* E **16** 528–32

[44] Elfving A, Karim A, Hansson G V and Ni W X 2006 Three-terminal Ge dot/SiGe quantum-well photodetectors for near-infrared light detection *Appl. Phys. Lett.* **89** 13–6

[45] Elkurdi M, Boucaud P, Sauvage S, Kermarrec O, Campidelli Y, Bensahel D, Saint-Girons G and Sagnes I 2002 Near-infrared waveguide photodetector with Ge/Si self-assembled quantum dots *Appl. Phys. Lett.* **80** 509–11

[46] Yakimov A I, Dvurechenskiĭ A V, Nikiforov A I, Chaĭkovskiĭ S V and Tiĭs S A 2003 Ge/Si photodiodes with embedded arrays of Ge quantum dots for the near infrared (1.3–1.5 μm) region *Semiconductors* **37** 1383–8

[47] Yu J, Kasper E and Oehme M 2006 1.55-μm resonant cavity enhanced photodiode based on MBE grown Ge quantum dots *Thin Solid Films* **508** 396–8